# Facile synthesis of $ZnO/BiVO_4$ photocatalyst with enhanced photocatalytic performance

YANHONG GUO, QIANGEN LI, XIAOMING GAO*, KAILONG GAO, LIBO LIU
*Department of Chemistry and Chemical Engineering, Shaanxi Key Laboratory of Chemical Reaction Engineering, Yan'an University, Yan'an, Shaanxi 716000, China*

To fabricate composite with narrow gap semiconductor are considered as a tactics for photocatalyst material with high ability. $ZnO/BiVO_4$ composite was hydrothermal synthesis, and the crystal structure and morphology was investigated by XRD, DRS, SEM and TEM. The photocatalytic activity of $ZnO/BiVO_4$ was examined by degradation of methylene blue and thiophene. The removal rate for methylene blue of 20wt% $ZnO/BiVO_4$ was 2.8 and 3.3 times than that of pristine ZnO and $BiVO_4$, respectively, and the desulfurization rate of model oil arrived at 97.4% after 120 min illumination. The synergistic effect of active oxidizing species involving in photocatalytic degradation process was researched in detail, with emphasized on the contribution of the hydroxyl free radical to the photocatalytic activity.

(Received January 21, 2019; accepted February 17, 2020)

*Keywords*: $ZnO/BiVO_4$ composite, Photocatalytic, Oxidation

## 1. Introduction

Photocatalytic technology has been extensively researched for addressing environmental pollution [1-3]. In this field, rationally fabricating photocatalyst with high-efficiency and outstanding light absorption became the driving force [4-6]. In recent years, $TiO_2$, was employed as catalyst for photocatalytic technology, have been the research focuses [7, 8]. However, $TiO_2$ not only required high excitation energy, but also absorbed ultraviolet light in the solar spectrum [9, 10]. Therefore, universal attempts have been made to develop $TiO_2$-based photocatalysts sensitive to visible light, such as dye sensitization, metal/nonmetal coupling, and so on [11-13]. However, merely inducing visible light absorption does not always result in the high-efficiency visible light photocatalytic activity [14-16]. Therefore, it is still a desirable issue to design and fabricate a novel photocatalyst with highly active under visible light irradiation [17-19].

Recently, bismuth vanadate ($BiVO_4$) has received interest because of its diversity of crystal structure and the electronic structure and high charge fluidity in response to visible light [18, 20]. However, $BiVO_4$ usually shows a relative low photocatalytic activity due to its rapid recombination of photogenerated carrier and weak photo absorption, thus limiting potential application of $BiVO_4$ as an effective photocatalyst [21, 22]. To this end, developing more effective $BiVO_4$ photocatalyst of wide photo-response range and low recombination rate of the photoinduced electron-hole pairs is of great importance. To inhibit recombination efficiency of carrier and extend light responsive range of $BiVO_4$, several strategies have been advanced, for example, nanostructured $BiVO_4$ with large specific surface area and coupling of metal/non-metal element. Particularly, we synthesized $BiVO_4$ photocatalyst via a hydrothermal method, and Ag or Nd nanoparticles was successfully deposited on the surface of $BiVO_4$ [23, 24]. Our results showed that doped $BiVO_4$ exhibited high efficiency for the photocatalytic degradation of phenol compared with unmodified $BiVO_4$. However, the dopants could readily form recombination centers for photoinduced electron-hole pairs, and the separating and migrating of photoinduced carriers is inhibited, thus leading to decrease in photocatalytic efficiency [25, 26]. Therefore, other more effective strategies should be developed to overcome this obstacle. Thus, to improve the photocatalytic activity, fabricated composite $BiVO_4$ with controlling morphology and coupling narrow gap semiconductor seems to be an effective means [27-30].

Herein, a series of $ZnO/BiVO_4$ composite was prepared via a hydrothermal synthesis method. The influence of combined proportion on the structural, crystallinity, surface areas and photo-response ability of $ZnO/BiVO_4$ were systematically discussed by several means. The photocatalytic activities were evaluated from MB degradation and thiophene oxidation under visible light. Finally, the related mechanisms were discussed in detail.

## 2. Experiment

### 2.1. Preparation

The solution contained 25 mmol $Zn(CH_3COO)_2$ $2H_2O$, 24 mmol NaOH and 50 mL ethanol was transferred into 100 mL Teflon-lined stainless vessel, which was heated to 160°C for 8h. After cooling to room temperature, the obtained sample was centrifuged and washed with distilled water. Afterwards, sample was obtained in a drying cabinet at 60°C for 4h, which were named as ZnO sample.

2 mmol $Bi(NO_3)_3 \cdot 5H_2O$ and 2 mmol $NH_4VO_3$ were dissolved in nitric acid and deionized water respectively. Subsequently, two solutions were mixed, added different amounts of ZnO samples with stirring for 30 min. Then, the mixture was transferred into 100 mL Teflon-lined stainless autoclave and heated at 160°C for 8h. After cooling to room temperature, the product was centrifuged and washed with distilled water, and dried at 80°C for 4h. The prepared samples were designated as 5wt% ZnO/$BiVO_4$, 10wt% ZnO/$BiVO_4$, 20 wt% ZnO/$BiVO_4$ and 30 wt% ZnO/$BiVO_4$ composite.

### 2.2. Characterization

The purity and crystallinity of samples were detected by Shimadzu XRD-7000 X-ray diffraction (XRD) using Cu $K_\alpha$, 40 kV, 100 mA. The microstructures of the samples were identified by Hitachi SU8010 field emission scanning electron microscopy (FE-SEM). High-resolution transmission electron (HR-TEM) of the samples was measured by JEM-2100 electron microscope with 200 kV of accelerating voltage. The optical property was recorded by Shimadzu UV-2550 UV–vis spectrophotometer with an integrating-sphere accessory, $BaSO_4$ as the standard. The chemical constitute of the as-prepared samples were analyzed using EDS (Bulker Q73). The photoinduced fluorescence spectra of samples was analysed by the fluorescence spectrometer (Hitachi F-4500). The electrochemical impedance spectroscopy were measured by in CHI660E electrochemical workstation with Pt electrode, saturated calomel electrode and graphite electrode containing sample.

### 2.3. Photocatalytic properties

100 mg photocatalysts and 50 mL MB-containing wastewater (20 mg/L) were added into quartz tube and stirred in dark for 1 h to ensure adsorption-desorption equilibrium. After that, the solution was illuminated by 400W metal halide with a 400 nm cut-off. During this period, 5 mL of sample were taken at given time intervals and the photocatalysts were separated through centrifugation. The MB concentration was determined from the spectrophotometric measurement.

Thiophene was dissolved in n-octane to form model oil with the sulfur concentration of 250 mg/g). 100 mg as-prepared photocatalysts, 50 mL of acetonitrile and 250 mL of model oil were transferred into quartz tube and then stirred in dark for 1h. After that, the solution was illuminated by 400 W metal halide with a 400 nm cut-off. During this period, 5 mL of sample were taken at given time intervals and the photocatalysts were separated through centrifugation. The total sulfur concentration in the n-octane phase was determined by Elemental Analyzer (trace SN cube Elementar, Germany).

## 3. Result and discussion

### 3.1. XRD

The purity and crystallinity of samples were examined by XRD measurements. As shown in Fig. 1, the diffraction peaks of the as-prepared sample are observed at 2θ = 18.3°, 24.4°, 30.7°, 32.7°, 34.7°, 39.5° and 48.4°, which can be corresponded to tetragonal phase of $BiVO_4$ (JCPDS No. 14-0133, $I4_1/amd$). These peaks were attributed to diffraction of (101), (200), (211), (112), (220), (301) and (312) crystal planes, respectively. Meanwhile, 2θ of 28.9°, 30.5°, 34.5°, 35.2°, 40.0°, 42.5°, 47.3°, 50.3° and 53.4° can be indexed to monoclinic phase (JCPDS No. 14-0688, Pnca (61)). These peaks were indexed to diffraction of (121), (040), (200), (002), (112), (051), (042), (202) and (310) planes, respectively. Among them, the strongest diffraction appears at 2θ = 34.4° for (002) plane, which was indexed to hexagonal ZnO (JCPDS No. 36-1451). In addition, no peak of other impurities is detected. The lattice parameters of the as-prepared samples are shown in Table 1. Neglectable change in the lattice parameters is found between $BiVO_4$ and ZnO/$BiVO_4$. In addition, with the increase of coupling content of ZnO, the intensity of characteristic peak at 2θ = 34.4° increases.

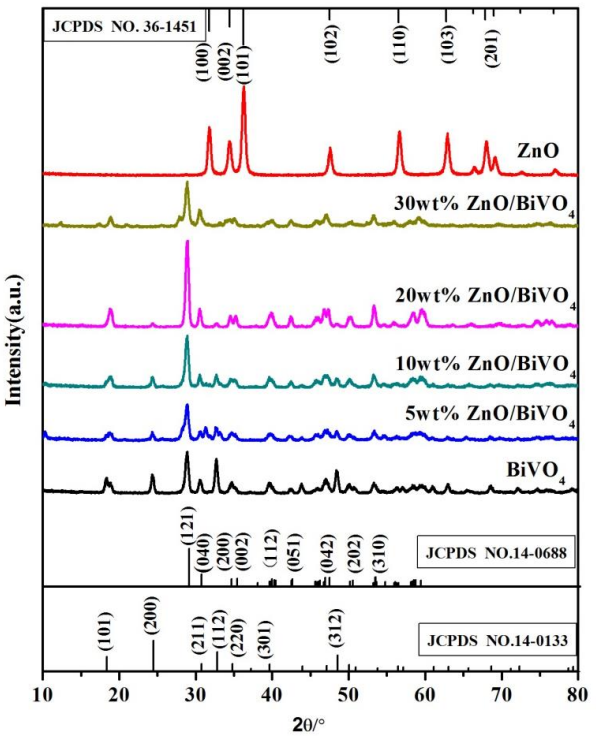


*Fig. 1. XRD analysis of the as-prepared samples (color online)*

To confirm the components of 20% $ZnO/BiVO_4$ composite, EDS of as-prepared samples was carried out as shown in Fig. 2. The diffraction peaks of Bi, V, Zn, and O elements corresponding to $ZnO/BiVO_4$ composite are observed. From insert table of Fig. 2, the experimental values of Bi, V, Zn, and O elements are close to the theoretical values for 20%$ZnO/BiVO_4$ composites. Furthermore, from Fig. 3, it could be drawn that O element were the most abundant, followed by Bi element and V element, which also confirmed the $BiVO_4$ as the main component. Zn element had the less content, which contributed to be a little addition in the preparation. In conclusion, the sample is composed of 20%$ZnO/BiVO_4$ composite.

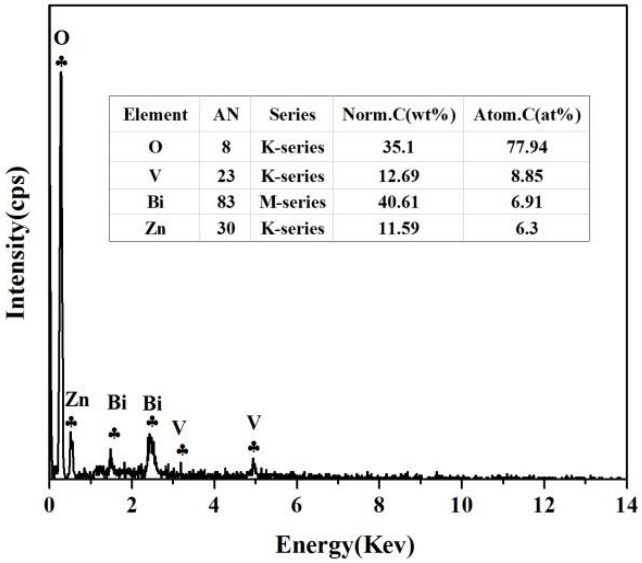


| Element | AN | Series | Norm.C(wt%) | Atom.C(at%) |
|---|---|---|---|---|
| O | 8 | K-series | 35.1 | 77.94 |
| V | 23 | K-series | 12.69 | 8.85 |
| Bi | 83 | M-series | 40.61 | 6.91 |
| Zn | 30 | K-series | 11.59 | 6.3 |

*Fig. 2. EDS of components of 20% $ZnO/BiVO_4$*

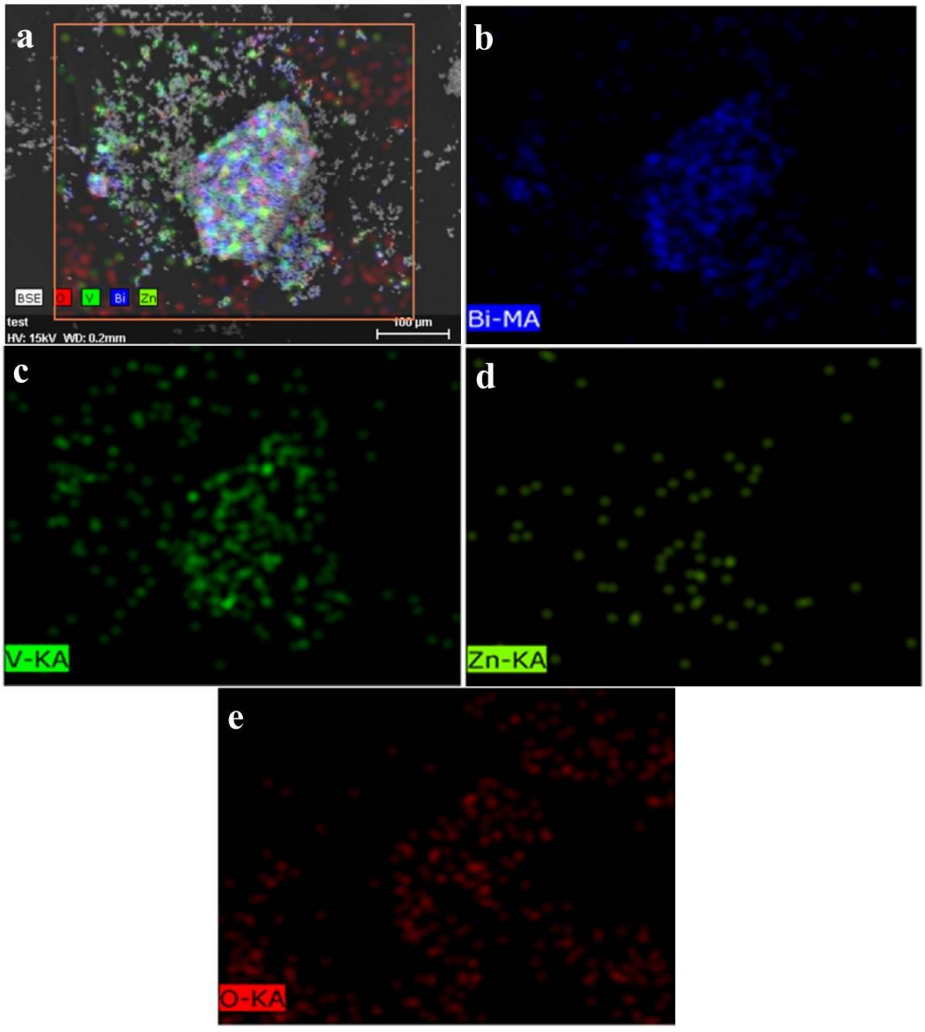


*Fig. 3. The mapping graph of 20%$ZnO/BiVO_4$ composite, (a) analysis area, the distribution of (b) Bi, (c) V, (d) Zn, (e) O (color online)*

### 3.2 Morphology and structure

Fig. 4 displays the morphology and microstructure of the as-prepared samples. A plate-like structure composite was observed as ZnO coupling amount of 5% (Fig. 4a). With increasing of ZnO amount, the ZnO particles were

dispersed on the surface of $BiVO_4$ particles. For 10% ZnO/$BiVO_4$, the ZnO particles uniformly were dispersed on the surface of $BiVO_4$ particles (Fig. 4b). As far as 20% ZnO/$BiVO_4$, ZnO and $BiVO_4$ were tightly combined (Fig. 4c). As the amount of ZnO is further increased to 30%, ZnO exhibited a rod-like structure (Fig. 4d).

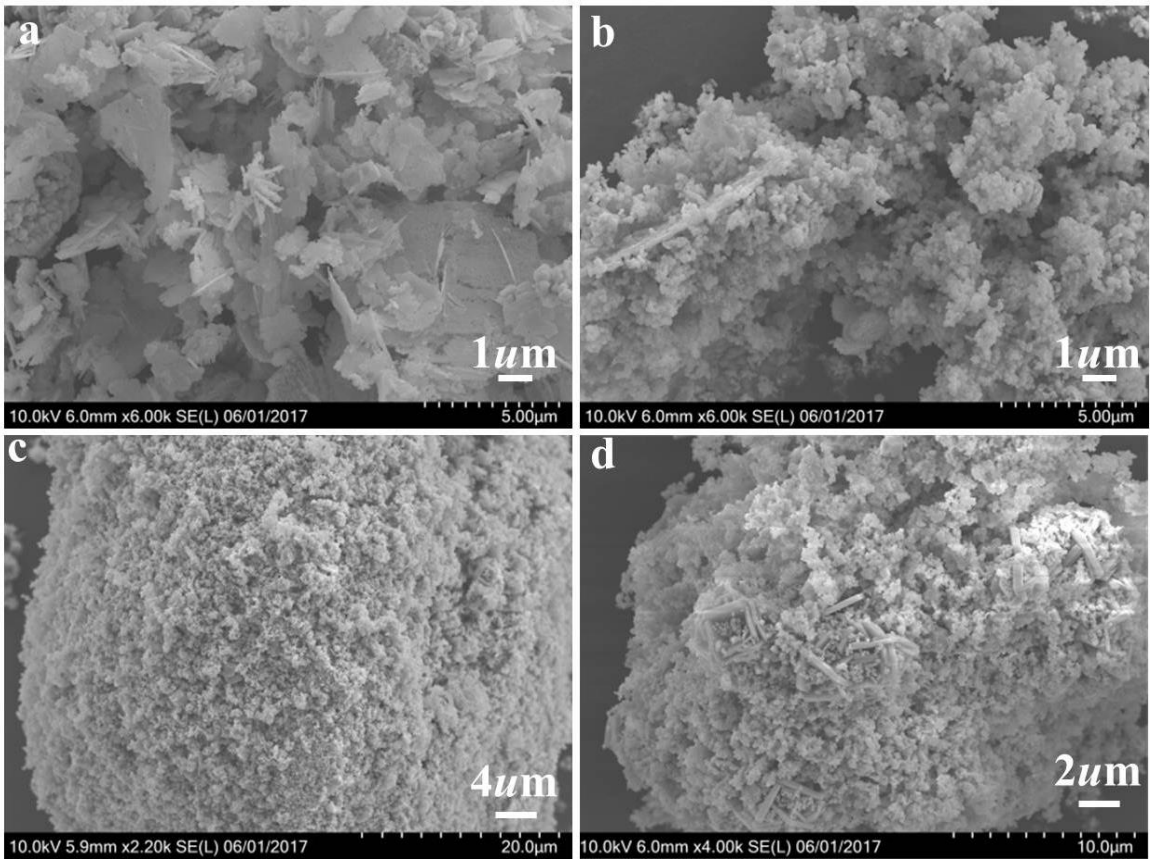


*Fig. 4. The FE-SEM patterns of the as-prepared samples (a) 5% ZnO/$BiVO_4$ (b) 10% ZnO/$BiVO_4$ (c) 20% ZnO/$BiVO_4$, (d) 30% ZnO/$BiVO_4$*

The microstructure and morphology of the as-prepared samples are further by TEM and HR-TEM analysis, as shown in Fig. 5. From Fig. 5(a), it can be clearly seen that an obvious phase interface was formed between ZnO and $BiVO_4$, which was well agree with the SEM results. As shown in Fig. 5b, there were two kinds of continuous lattice fringes of the representative particle in the selected region: the continuous lattice fringes with a d-spacing of 0.36 nm can be perfectly indexed to (121) planes of the monoclinic phase of $BiVO_4$, while the continuous lattice fringes with a d-spacing of 0.25 nm agreed well with (222) planes of the hexagonal ZnO.

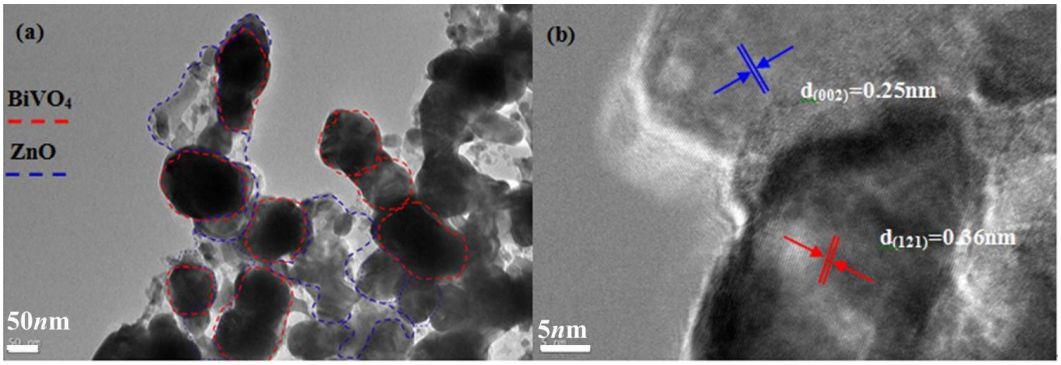


*Fig. 5 (a) TEM image, and (b) HR-TEM image of 20%ZnO/$BiVO_4$ composite*

### 3.3. UV-vis DRS

The optical absorption property of the as-prepared samples was studied by UV-Vis DRS. As shown in Fig. 6, the as-prepared samples possessed excellent light-harvesting from the UV to visible light region. Compared with absorption ranging from 500 to 700 nm of pristine ZnO and $BiVO_4$, $ZnO/BiVO_4$ presented a red shift enhancement as the increasing of coupling content of $BiVO_4$. The red shift of absorption edge indicated the increasing of absorption ability of visible light. Especially, 20% $ZnO/BiVO_4$ displays an additional and strong visible light absorption around 570-700 nm, demonstrating the potential application as high-effective visible light photocatalysts. The band gap energy (eV) can be calculated using the equation $Ahv = c\ (hv - Eg)^n$ from the diffuse reflection spectral data[31]. The band gap energy estimated from the intercept of the tangents to the plots are 2.5, 3.1, 2.48, 2.3, 2.3 and 2.7 eV for samples of pure $BiVO_4$, ZnO, 5%$ZnO/BiVO_4$, 10%$ZnO/BiVO_4$, 20%$ZnO/BiVO_4$ and 30%$ZnO/BiVO_4$ composites respectively (Fig. 7).

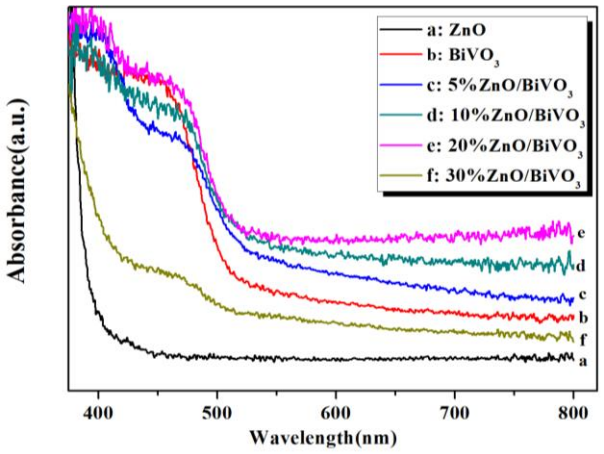


*Fig. 6. UV-vis DRS of the as-prepared samples (color online)*

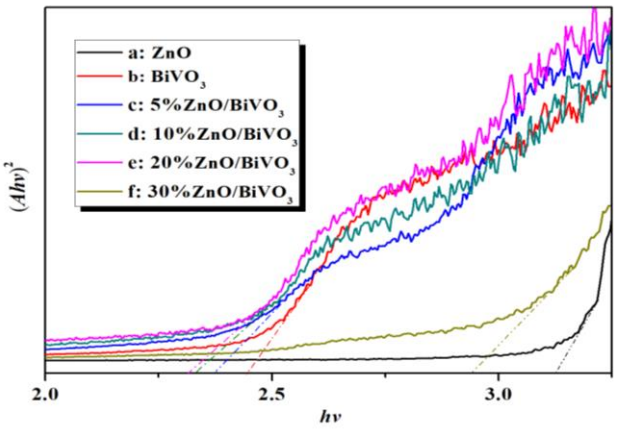


*Fig. 7. Eg of the as-prepared samples (color online)*

### 3.4. Photocatalytic property

The photocatalytic activity of the as-prepared samples was examined by MB degradation under 400W metal halide with a cut off light below 400 nm. As shown in Fig. 8, with the prolonging of illumination time, MB can be decomposed without photocatalyst, but the degradation efficiency is lower than 10%. However, the degradation efficiency was improved with adding of photocatalyst. After 105 min of illumination, in the presence of $BiVO_4$ and ZnO, the degradation rate can reach to 42.5%, 16.7%, respectively. Nevertheless, the MB removal rate of 74.9%, 86%, 91.5%, 68.1% for 5% $ZnO/BiVO_4$, 10% $ZnO/BiVO_4$, 20% $ZnO/BiVO_4$ and 30% $ZnO/BiVO_4$ is obtained, respectively. Therefore, MB can be degraded more efficiently using $ZnO/BiVO_4$.

Further analyzing MB concentration with time, the result obeyed the pseudo-first order kinetics model, $\ln(c_0/c) = kt$. As shown in Fig. 9, the apparent rate constant $k$ is calculated to be 0.00824 $min^{-1}$, 0.0071 $min^{-1}$, 0.01302 $min^{-1}$, 0.01876 $min^{-1}$, 0.02342 $min^{-1}$ and 0.01096$min^{-1}$ for pure ZnO, pure $BiVO_4$ and 5% $ZnO/BiVO_4$, 10% $ZnO/BiVO_4$, 20% $ZnO/BiVO_4$, 30% $ZnO/BiVO_4$, respectively. Remarkably, the photocatalytic reaction rate of 20% $ZnO/BiVO_4$ was about 2.8 times faster than that of pure ZnO, and 3.3 times faster than that of $BiVO_4$. In order to confirm mineralization of MB, the change of the total organic carbon was ascertained by TOC analyzer. According to Fig. 10, the TOC value of MB solution over 20% $ZnO/BiVO_4$ reached to 87.5% after irradiated 90 min, indicating that the possible mineralization of MB by $ZnO/BiVO_4$ composites was happened. Deva Kumar[32] reported that $ZnO/BiVO_4$ composite (theoretical mass percentage of $BiVO_4$ in ZnO was 24.8%) had 64% reduction in COD for simulated tannery industry wastewater in six hours of reaction in the presence of sun light.

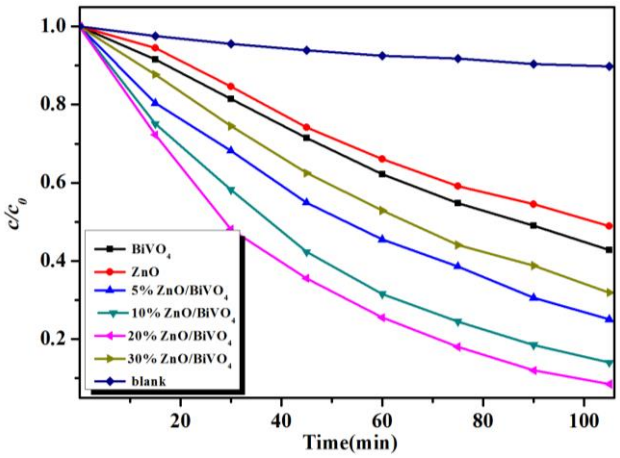


*Fig. 8. The degradation effect of MB over the as-prepared samples (color online)*

Fig. 11 shows the photocatalytic desulfurization activities of the as-prepared samples. As shown in Fig. 11, thiophene is almost oxidatively degraded without photocatalyst under visible illumination. Nevertheless, the desulfurization efficiency is increased evidently with addition of ZnO and $BiVO_4$, and the removal rate reaches to 38.2% and 37.8% after irradiated 120 min, respectively. Moreover, the desulfurization rate of model oil with 20% $ZnO/BiVO_4$ composite arrived at 97.4%.

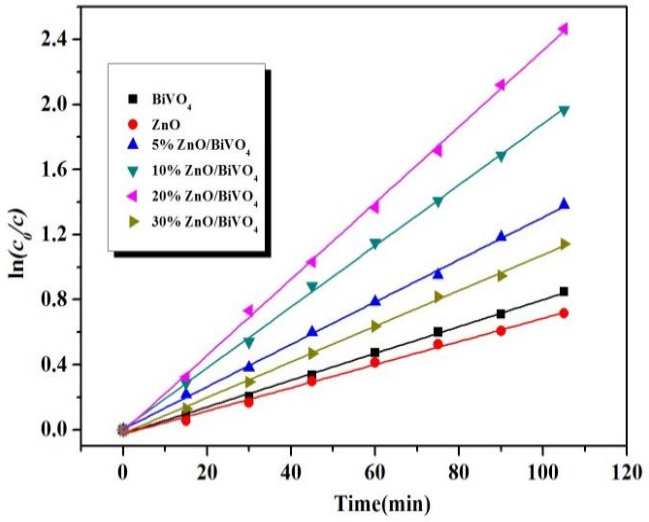


*Fig. 9. Kinetic linear simulation curve of photodegradation MB with the as-prepared samples (color online)*

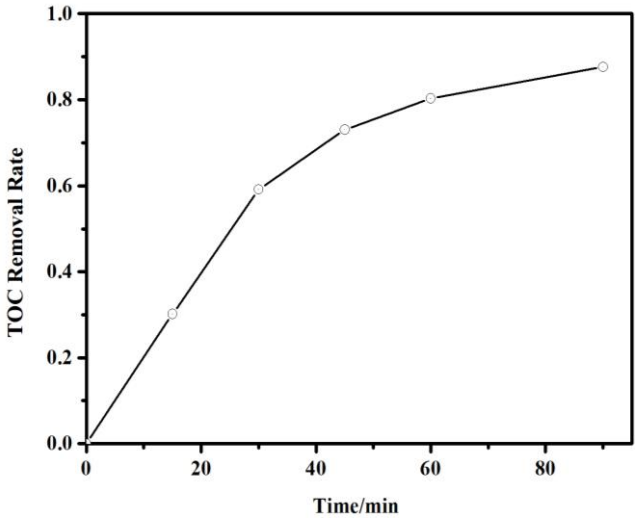


*Fig. 10. TOC changes of MB solution over 20% $ZnO/BiVO_4$*

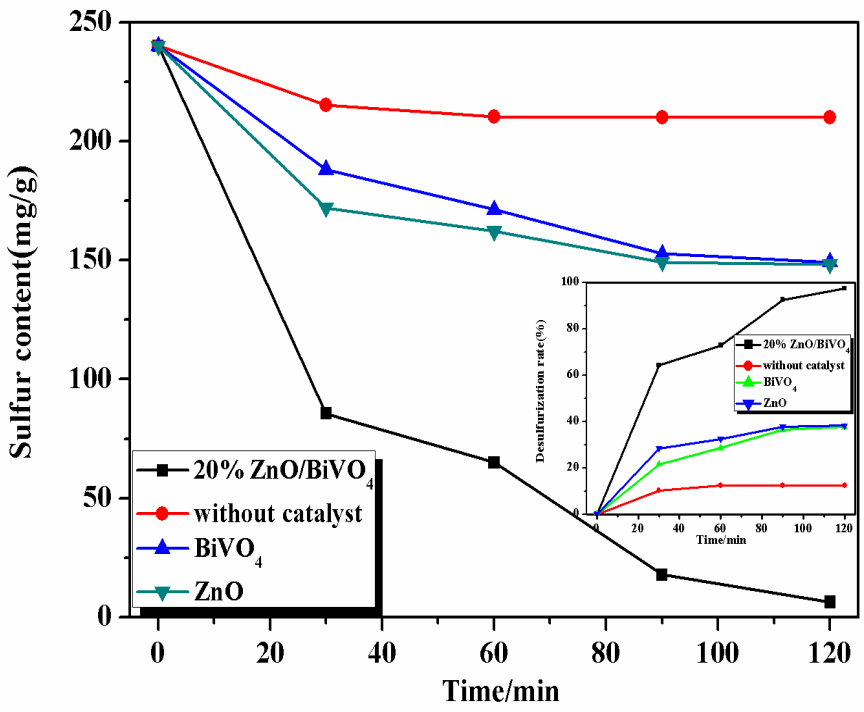


*Fig. 11. Photocatalytic desulfurization activity and the desulfurization rate of the as-prepared samples under visible-light irradiation (inset) (color online)*

The electrochemical impedance spectroscopy (EIS) of 20% $ZnO/BiVO_4$, ZnO and $BiVO_4$ was determined by CHI600A electrochemical workstation, and the result is shown in Fig. 12. The radius of the arc on the EIS is related to the separation rate of photogenerated electrons and holes, and concerned with the interface layer resistance. A smaller arc radius implies a higher separation rate of the photogenerated electron-hole pairs, and higher efficiency of charge transfer [33, 34]. So, the interface charge separation efficiency of 20% $ZnO/BiVO_4$, ZnO and

$BiVO_4$ can be indirectly determined by the EIS spectrum. According to Fig. 11, the arc radius of 20% $ZnO/BiVO_4$ is smaller than that of ZnO and $BiVO_4$. The result indicated that 20% $ZnO/BiVO_4$ presented dramatically enhancement of the separation and transfer efficiency of charge carriers through an interfacial interaction between ZnO and $BiVO_4$, which is consistent with the photocatalytic degradation result.

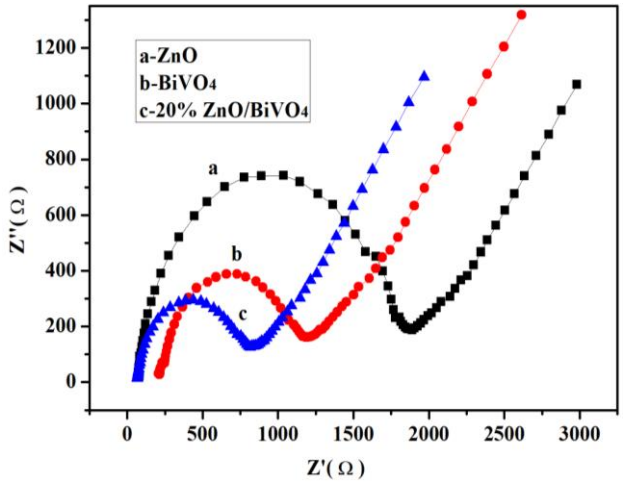


*Fig. 12. EIS spectrum of the as-prepared samples with light on/off cycles under the visible light (λ> 420 nm) (color online)*

As shown in Fig. 13, under the same excitation wavelength, ZnO exhibits strong photoluminescence peak at 390 nm, and $BiVO_4$ shows strong photoluminescence peak at 376 nm. However, compared to ZnO and $BiVO_4$, the strength of the emission peak of $ZnO/BiVO_4$ is significantly reduced. Therefore, the recombination of charge carrier could be effectively inhibited in 20% $ZnO/BiVO_4$ composite, which owing to a fraction of holes in the $BiVO_4$ transfer to ZnO. The result was accorded with the photocatalytic degradation.

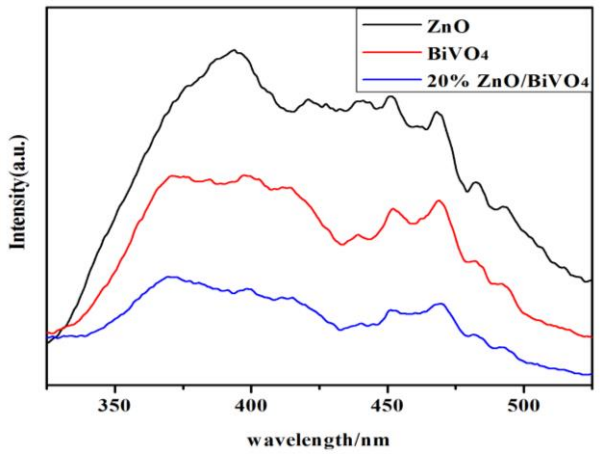


*Fig. 13. The Fluorescence of 20% $ZnO/BiVO_4$, ZnO and $BiVO_4$ (color online)*

To determine the function of the active free radicals, the MB degradation experiments were carried out in the presence of different scavengers (i.e., benzoquinone (BQ), ethylene diamine tetra-acetic acid (EDTA) and isopropanol (IPA) [32, 35] over 20% $ZnO/BiVO_4$. As shown in Fig. 14, without any scavengers, the degradation rate is 90.6% in 90 min. With the adding of BQ, the degradation rate decreases significantly, because of capturing of the superoxide radical anion $O_2^-$•, a strong oxidize species. Therefore, in this case the MB degradation rate of is only 50.2%. $O_2^-$• played an important role in the photocatalytic oxidation degradation. Meanwhile, the degradation rate also decreases as the adding of EDTA, due to the capturing of the photo-generated hole $h^+$, which leaded to the degradation rate of 58.3%. So, photo-generated hole $h^+$ is an important oxidant for the photocatalytic degradation. However, the addition of IPA inhibited MB degradation even further, indicating important effect of the hydroxyl free radical •OH. The MB degradation was promoted mainly by •OH, and $O_2^-$• and $h^+$ also play a positive role in the process.

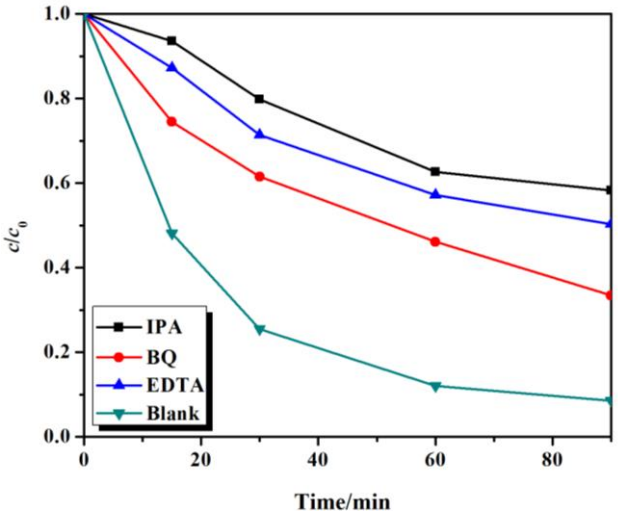


*Fig. 14. Effect of scavengers on photocatalytic activity of 20%$ZnO/BiVO_4$ under visible light (color online)*

## 4. Conclusions

The $ZnO/BiVO_4$ composite with enhanced activity was synthesized via a facile hydrothermal method. $ZnO/BiVO_4$ showed controlled morphology, high crystallinity and high absorption intensity. The photocatalytic activity of $ZnO/BiVO_4$ composite was greatly enhanced compared with pristine ZnO and pure $BiVO_4$. The radicals trapping experiments suggested that hydroxyl free radical •OH was the key reactive species for the photocatalytic degradation. The enhanced photoactivity was attributed to a synergistic effect of the inhibited recombination of charge carriers, the increased absorption of visible light and surface hydroxyl free radicals.

**Acknowledgments**

This work has received the finical support from the National Natural Science Foundation of China (Grant No. 21766039), the Major Project of Yanan Science and Technology Bureau (Grant No. 2016CGZH-10).

## References

[1] C. Pan, Y. Zhu, Cata. Sci. Technol. **5**, 3071 (2015).
[2] X. Y. Liu, H. Chen, R. Wang, Y. Shang, Q. Zhang, W. Li, G. Zhang, J. Su, C. T. Dinh, F. P. G. de Arquer, J. Li, J. Jiang, Q. Mi, R. Si, X. Li, Y. Sun, Y.-T. Long, H. Tian, E. H. Sargent, Z. Ning, Adv. Mater. **29**, 1605646 (2017).
[3] S. Dong, L. Xia, T. Guo, F. Zhang, L. Cui, X. Su, D. Wang, W. Guo, J. Sun, Appl. Surf. Sci. **445**, 30 (2018).
[4] H. I. Kim, S. Weon, H. Kang, A. L. Hagstrom, O. S. Kwon, Y. S. Lee, W. Choi, J.-H. Kim, Environ. Sci. Technol. **50**, 11184 (2016).
[5] X. Lu, W. Che, X. Hu, Y. Wang, A. Zhang, F. Deng, S. Luo, D. D. Dionysiou, Chem. Eng. J. **356**, 819 (2019).
[6] X. Li, J. Xiong, J. Huang, Z. Feng, J. Luo, J. Alloy. Compd. **774**, 768 (2019).
[7] H. Wang, L. Zhang, Z. Chen, J. Hu, S. Li, Z. Wang, J. Liu, X. Wang, Chem. Soc. Rev. **43**, 5234 (2014).
[8] J. Tian, Z. Zhao, A. Kumar, R. I. Boughton, H. Liu, Chem. Soc. Rev. **43**, 6920 (2014).
[9] H. Park, H. I. Kim, G. H. Moon, W. Choi, Energ. Environ. Sci. **9**, 411 (2016).
[10] J. Kim, J. Kim, Environ. Sci. Technol. **48**, 13384 (2014).
[11] P. G. Smirniotis, T. Boningari, D. Damma, S. N. R. Inturi, Catal. Commun. **113**, 1 (2018).
[12] V. Iliev, D. Tomova, L. Bilyarska, J. Photoch. Photobio. A **351**, 69 (2018).
[13] Y. Huang, S. Kang, Y. Yang, H. Qin, Z. Ni, S. Yang, X. Li, Appl. Catal. B: Environ. **196**, 89 (2016).
[14] E. T. Yun, H. Y. Yoo, W. Kim, H. E. Kim, G. Kang, H. Lee, S. Lee, T. Park, C. Lee, J. H. Kim, J. Lee, Appl. Catal. B: Environ. **203**, 475 (2017).
[15] L. Hao, H. Huang, Y. Guo, Y. Zhang, ACS Sustain. Chem. Eng. **6**, 1848 (2018).
[16] X. Gao, K. Gao, F. Fu, C. Liang, Q. Li, J. Liu, L. Gao, Y. Zhu, Appl. Catal. B: Environ. **265**, 118562 (2020).
[17] Y. Yang, Z. Zeng, C. Zhang, D. Huang, G. Zeng, R. Xiao, C. Lai, C. Zhou, H. Guo, W. Xue, M. Cheng, W. Wang, J. Wang, Chem. Eng. J. **349**, 808 (2018).
[18] Z.-F. Huang, L. Pan, J.-J. Zou, X. Zhang, L. Wang, Nanoscale **6**, 14044 (2014).
[19] X. Li, J. Xiong, Y. Xu, Z. Feng, J. Huang, Chin. J. Catal. **40**, 424 (2019).
[20] C. Regmi, Y. K. Kshetri, T. H. Kim, R. P. Pandey, S. K. Ray, S. W. Lee, Appl. Surf. Sci. **413**, 253 (2017).
[21] Q. Wang, J. He, Y. Shi, S. Zhang, T. Niu, H. She, Y. Bi, Chem. Eng. J. **326**, 411 (2017).
[22] W. Fang, Z. Jiang, L. Yu, H. Liu, W. Shangguan, C. Terashima, A. Fujishima, J. Catal. **352**, 155 (2017).
[23] X. Gao, Z. Wang, X. Zhai, F. Fu, W. Li, J. Mole. Liq. **211**, 25 (2015).
[24] R. Sun, Q. Shi, M. Zhang, L. Xie, J. Chen, X. Yang, M. Chen, W. Zhao, J. Alloy. Compd. **714**, 619 (2017).
[25] P. Li, X. Chen, H. He, X. Zhou, Y. Zhou, Z. Zou, Adv. Mater. **30**, 1703119 (2018).
[26] L. Zhang, A. A. S. Gonçalves, B. Jiang, M. Jaroniec, Chem. Sus. Chem. **11**, 1486 (2018).
[27] H. S. Park, C. Y. Lee, E. Reisner, Phys. Chem. Chem. Phys. **16**, 22462 (2014).
[28] L. S. Zhang, K. H. Wong, H. Y. Yip, C. Hu, J. C. Yu, C. Y. Chan, P. K. Wong, Environ. Sci. Technol. **44**, 1392 (2010).
[29] G. Colón, S. Murcia López, M. C. Hidalgo, J. A. Navío, Chem. Comm. **46**, 4809 (2010).
[30] Z. Yi, Q. Han, P. Zan, Y. Cheng, Y. Wu, L. Wang, J. Mater. Chem. A **4**, 12850 (2016).
[31] W. Kubo, T. Tatsuma, J. Am. Chem. Soc. **128**, 16034 (2006).
[32] E. T. D. Kumar, K. Thirumalai, S. Balachandran, R. Aravindhan, M. Swaminathan, J. Raghava Rao, Surf. Interf. **8**, 147 (2017).
[33] S. Dong, X. Ding, T. Guo, X. Yue, X. Han, J. Sun, Chem. Eng. J. **316**, 778 (2017).
[34] X. Gao, Y. Shang, L. Liu, F. Fu, J. Catal. **371**, 71 (2019).
[35] H. Tian, M. Liu, W. Zheng, Appl. Catal. B: Environ. **225**, 468 (2018).

*Corresponding author: dawn1026@163.com